Journal of Alloys and Compounds 509 (2011) 2407–2413

Contents lists available at ScienceDirect

Journal of Alloys and Compounds

journal homepage: www.elsevier.com/locate/jallcom

Formation and calcination temperature-dependent sintering activity of YAG precursor synthesized via reverse titration method

Yuanhua Sang[a], Hong Liu[a,*], Xudong Sun[b,**], Xiaolin Zhang[a], Haiming Qin[a], Yaohui Lv[a], Di Huo[b], Duo Liu[a], Jiyang Wang[a], Robert I. Boughton[c]

[a] State Key Laboratory of Crystal Materials, Shandong University, 27 Shandanan Road, Jinan 250100, China
[b] School of Materials and Metallurgy, Northeastern University, Shenyang, 110004, China
[c] Center for Material Science, Bowling Green State University, Bowling Green, OH 43403, USA

ARTICLE INFO

Article history:
Received 28 June 2010
Received in revised form 2 November 2010
Accepted 4 November 2010
Available online 13 November 2010

Keywords:
Precipitation
Grain boundaries
Scanning and transmission electron microscopy

ABSTRACT

The composition homogeneity of YAG precursors synthesized via both normal and reverse titration co-precipitation methods is discussed. It was demonstrated that that the reverse titration process possesses better co-precipitation characteristics than the normal titration process, based on a real-time monitoring of the reaction pH and measurement of the Y/Al ratio in the precipitate. The formation process of the precipitate obtained by reverse titration method was discussed. The effect of calcination temperature on sintering properties of the YAG powder was investigated by analysis of the crystalline phase, the specific surface area, and the morphology of the powder. The shrinkage rate test of compacts made from different powders indicates that a higher calcination temperature results in a lower densification speed and shrinkage ratios. Microstructure observation shows that the ceramics made from YAG nanopowder, which was obtained at a higher calcination temperature, have a more uniform grain-size distribution and fewer residual pores.

© 2010 Elsevier B.V. All rights reserved.

1. Introduction

Neodymium-doped yttrium aluminum garnet ($Y_{3-x}Nd_xAl_5O_{12}$, YAG) is widely used for laser applications. It is difficult to homogeneously dope over 1 at.% Nd as a luminescence element in a YAG single crystal [1], because of the low effective segregation coefficient of elemental Nd in YAG (about 0.2). However, this problem could possibly be solved by ceramic technology due to the high tolerance of defects and small grain size. Since the first demonstration of a Nd:YAG ceramic laser by Ikesue et al. in 1995 [2], significant progress in producing transparent YAG ceramics has been made. Many kinds of wet chemical routes were used for the preparation of fine powders for the ceramics sintering, such as all kinds of sol–gel methods [3–5], homogeneous precipitation [6,7], solvothermal [8–11] and supercritical water synthesis [12–14]. Especially, Yanagitani et al. proposed a process of fabricating the transparent YAG ceramics with phase pure YAG nanopowders [15–17]. Since then the ceramics have been able to exhibit a laser output of over 1460 W. As a result, the co-precipitation method with ammonium hydrogen carbonate as the precipitant became one of the favored processes for the preparation of YAG nanopowder [18–23]. The co-precipitation methods can mainly be generally divided into two kinds according to the sequence of reactants combination; one is the normal titration co-precipitation process [24], in which the precipitant solution is dropped into a mixed solution of the component cations to obtain the precipitate, and the other is the reverse titration co-precipitation process, in which the mixed cation solution is dropped into the precipitant solution. Researchers have deduced that composition homogeneity of the YAG precursor obtained by reverse titration is better than that from normal titration co-precipitation process, because of the difference in the solubility products of Y^{3+} and Al^{3+}. So far, there is no evidence to support the precipitation mechanism of the YAG precursor or any explanation of the dependence of cation homogeneity on different co-precipitation processes. In addition, the formation process of the precipitate obtained by the reverse titration process has not been discussed in detail. As is well known, fabrication of YAG powders is a complex process. Many factors, such as reaction temperature, final pH values [24], period of aging, and dosage of ammonium sulfate, would affect composition, morphology, and the final properties of the precursor. Moreover, the calcination process is also another important factor that affects sintering properties of the YAG powder. The effects of the calcination temperature have been emphasized for a long time. The two opposing views exist with regard to whether it is better to calcine the precursor at a high temperature to make the powder less sintering reactive, through particle growth [21,25], or to cal-

* Corresponding author. Fax: +86 531 88362807.
** Corresponding author.
E-mail address: hongliu@sdu.edu.cn (H. Liu).

0925-8388/$ – see front matter © 2010 Elsevier B.V. All rights reserved.
doi:10.1016/j.jallcom.2010.11.031

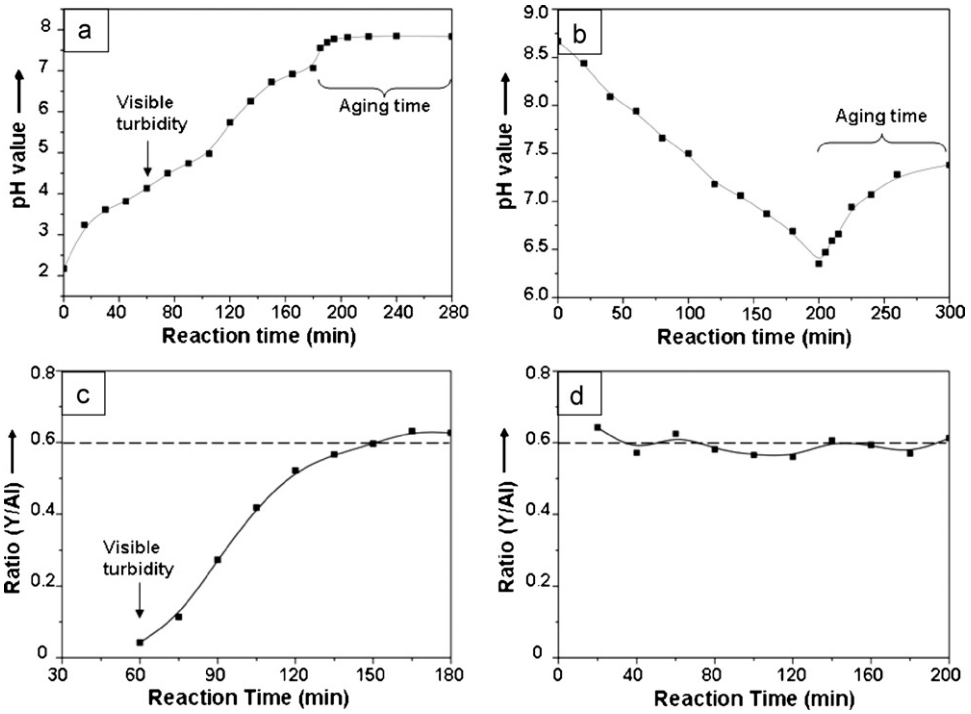

Fig. 1. Variation of pH and Y/Al ratio of the precipitate; (a and c) the normal titration co-precipitation method, (b and d) the reverse titration co-precipitation method.

cine it at a low temperature to retain high sintering activity [26,27]. In this work, the co-precipitation reaction mechanism was examined by making in situ measurements of the pH and checking the Y/Al ratios of the precipitate with an inductively coupled plasma emission spectrometer (ICP-AES). Moreover, the phase composition, particle size and morphology, and sintering behavior of the YAG powders calcined at different temperatures were investigated. Combined with microstructures observation of the sintered ceramics, it is shown that a higher calcination temperature is beneficial to sintering properties of the YAG powders.

2. Experimental procedures

Y_2O_3, Nd_2O_3 (Alfa Aesar, 99.99%) and $Al(NO_3)_3{\cdot}9H_2O$ (Alfa Aesar, 99.99%) were dissolved in HNO_3 (Sinopharm Chemical Reagent Co., Ltd., Specpure) and deionized water, respectively. These solutions were mixed to according to a stoichiometric cation ratio of $Y_{3-x}Nd_xAl_5O_{12}$ ($x=0$ for the ICP-AES analysis, and $x=0.6$ for the ceramic fabrication, 0.4 mol/L). 0.5 wt% of tetraethyl orthosilicate (TEOS) was added to the precipitant solution as a sintering aid. Ammonium hydrogen carbonate (Sinopharm Chemical Reagent Co., Ltd., AR) was dissolved in deionized water to obtain a precipitant solution of 2 mol/L. To investigate the difference between the two different co-precipitation modes, one group of samples were synthesized via normal titration, that is, the precipitant was dropped into the mother solution at a speed of 1.9 mL/min (marked as set 1), and another group of samples was synthesized via reverse titration by dropping the mother solution into the precipitant solution at a speed of 1.6 mL/min (marked as set 2). The change in the pH was recorded during the dropwise addition process at specific times. The Y/Al ratios in the precipitate were analyzed by regularly taking suspension samples (about 2 mL out of a total of between 340 mL and 660 mL) during the two different co-precipitation processes. The precipitate was washed with deionized water, and then dissolved in dilute HNO_3 with an ionic concentration of about 10 ppm before making the ICP-AES test. To study of the effects of calcination temperature on the sintering properties, Nd:YAG precursors were prepared using the same method as with set 2. After being filtered, washed and dried, the precursors were calcined at different temperatures in the range of 900–1300 °C for 2 h to obtain YAG powders, which were used for characterization of the phase composition, particle size and morphology, and for the measurement of sintering properties. After being compacted under an axial pressure of 200 MPa, some of the resultant pellets (Ø 8 mm, thickness > 4 mm) were used to test the shrinkage behavior, and others (Ø 13 mm) were sintered at 1700 °C for 10 h in vacuum.

The pH of the suspension was monitored with a pH meter (MP220 pH meter, Mettler-Toledo GmbH, Schwerzenbach, Switzerland). The concentrations of the yttrium and aluminum ions in the samples were determined with an inductively coupled plasma emission spectrometer (ICP-AES, IRIS Intrepid II XSP, Thermo Electron Corporation, USA). The BET surface area of the powders calcined at different temperatures was measured by an ASAP 2020 micropore physisorption analyzer (Micromeritics, USA). X-ray diffraction (XRD) patterns of the calcined powder were recorded by X-ray diffraction spectrometer (D8-advance, BrukerAXS, Germany). The shrinkage ratio of the compacts was tested with a thermal expansion apparatus (Setsys Evolution-24, Setaram, France) up to 1600 °C in nitrogen. Field emission scanning electron microscope (FESEM) images of the samples (both the powders calcined at different temperatures and the ceramics grain boundaries after thermally etched at 1450 °C for 4 h) were taken on a Hitachi S-4800 high resolution scanning electron microscope. Transmission electron microscope (TEM) image was taken on a JEM-2100 high resolution transmission electron microscope. Sample of 1.1 mm thick and mirror polished on both surfaces was used to measure the optical transmittance (Model U-4100 Spectrophotometer, Hitachi, Japan).

3. Results and discussion

3.1. Discussion of the precipitation processes

The recorded pH of the reaction system for both sets of 1 and 2 are shown in Fig. 1(a) and (b). The pH for both the reaction processes varies during the titration process, but approach a stable value in the aging process after the titration process termination. For set 1, the initial pH of the mother solution is about 2, which is caused by the excess nitric acid. The pH of the system increases with increase in the number of drops of NH_4HCO_3 (Fig. 1(a)). Turbidity is observed until the pH reaches 4.26. The pH increases further as the dropping process continues, and reaches a value of 7 at the end of the titration process. The system reaches its highest pH within a very short time (about 20 min) after termination of the titration process, and stabilizes at a constant pH of 7.84 during the aging period. In comparison with set 1, for set 2, the original pH is about 8.7, which reflects the pH of 2 mol/L ammonium hydrogen carbonate solution. The pH of the reaction system (Fig. 1(b)) shows a linear decrease during the titration process, and reaches a minimum value of 6.35 at termination. Then, the pH increases slowly (about 100 min before stabilization) as the aging process proceeds. The final pH is around 7.59 after aging for one day.

The variations of the Y/Al ratios of the precipitate, which were taken from the reaction system during both the co-precipitation processes, are shown in Fig. 1(c) and (d). An apparent variation of the Y/Al ratio in the precipitate during the titration process is observed in set 1 (Fig. 1(c)). The Y/Al ratio in the precipitate is as low as 0.05 at the first appearance of turbidity, which increases with the addition of ammonium hydrogen carbonate, and reaches a value of about 0.6 at the end of the titration process. For set 1, taking into account of the pH results (Fig. 1(a)), the regularity in the variation of the Y/Al ratio in Fig. 2(c) indicates that the Al^{3+} ions in the system settle down first, and Y-precipitate forms gradually with increasing pH during the normal co-precipitation process. When the pH reaches about 4, the Al-precipitate forms first [28], and makes the visibly turbid solution appear like a sol. A small amount of Y-precipitate forms under these conditions due to the high solubility product of Y^{3+}. With the increase in pH, more Y-precipitate forms, and adheres to the surface of the existing Al-precipitate, forming the YAG precursor precipitate. This process is referred to as differential precipitation. Finally, the Y/Al ratio in the precipitate reaches the stoichiometric value, because both the Y^{3+} and Al^{3+} cations are completely precipitated out. However, at the beginning of the reaction, the separation of Al- and Y-precipitates leads to inhomogeneous distribution of elemental yttrium and aluminum on a considerably large scale. The formation of YAG precursors is quite similar to the precipitation process using the urea method [28]. In the contrast, the reverse titration process provides a different precipitation avenue. Fig. 1(d) shows the variation of the Y/Al ratio, as a function of titration time, during the reverse titration co-precipitation process. At the beginning, the Y/Al ratio of the precipitate is about 0.6, consistent with the prescribed ratio of the mother solution, which is different from the case of normal titration. The Y/Al ratio of the precipitate maintains constant at 0.6 during the entire process. As shown in Fig. 1(b), the pH of the reaction system is over 8.5 at the beginning of titration. When the mother solution is dropped into the ammonium hydrogen carbonate solution, both Y and Al precipitate at the same time. This is

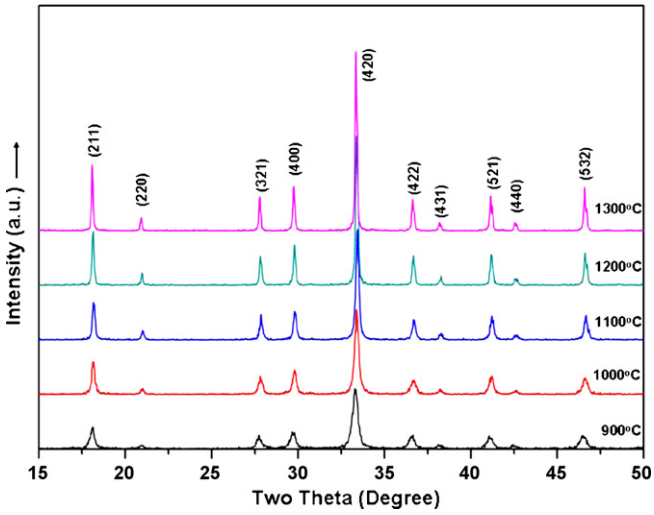

Fig. 2. XRD patterns of powder obtained by calcination at various temperatures for 2 h.

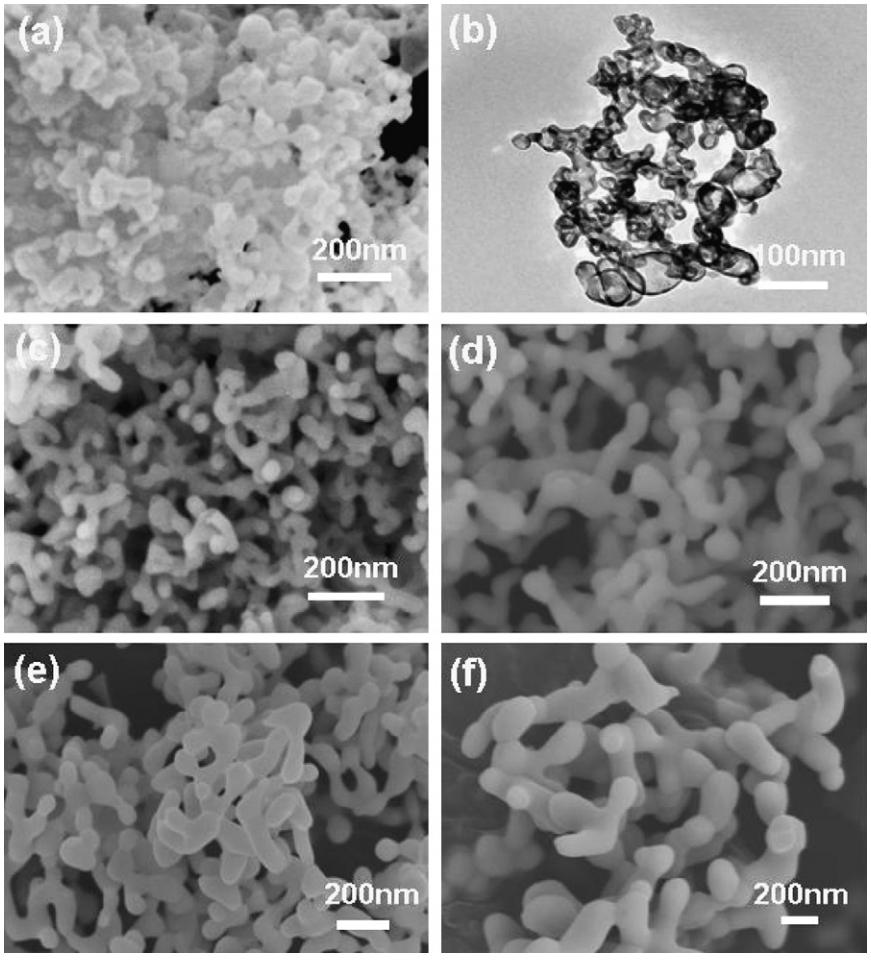

Fig. 3. . SEM and TEM images of powder obtained by calcination at different temperatures; (a and b) 900 °C, (c) 1000 °C, (d) 1100 °C, (e) 1200 °C, (f) 1300 °C.

because the pH is above the value needed for precipitation of both the cations. The sequence represents a genuine co-precipitation process. The linear variation of the pH during the titration indicates a steady depletion of NH_4HCO_3, which means the precipitation process proceeds in a steady fashion. Considering the stable Y/Al ratio in the precipitate, the ions distribution in the precipitate of set 2 should be homogenous during the entire process, no matter they precipitate at the beginning or at the end. However, the pH in a local region undergoes a change near the droplet. Regard the droplet and its neighborhood as a small reaction system. The reaction process should be quite similar to that of set 1 made via the normal titration co-precipitation method. The aluminum compound is assumed to form a core and is then coated by the yttrium compound, and form tiny primary particles in the neighborhood of the droplet. Driven by high surface energy and electrostatic attraction, these tiny particles combine and form the final precipitate. Because a pH gradient exists over a very small scale, the core of the Al-precipitate is assumed to be quite small, so the Y-precipitate can coat it well, and form a core–shell structure. As mentioned before, the restoration speed of the pH during the aging period is quite different between sets 1 and 2. The increases in pH are considered as the decomposition of carbonic acid and the consuming process of NH_4^+ to form a better crystallized compound of $NH_4Al(OH)_2CO_3$ [22,29], thus leaving more OH^- in solutions. The smaller increase in speed for set 2 partly implies that the aluminum compounds are better coated by the yttrium compounds, and thus more strongly retard the consumption of NH_4^+. On the other hand, the Al-precipitate particles in set 1 are too big to be well-coated by the Y-precipitate, and the pH approaches a constant value after a short time. The difference between the final pH values is due to the formation of different aluminum compounds under low pH condition, which consequently consumes a smaller amount of NH_4HCO_3.

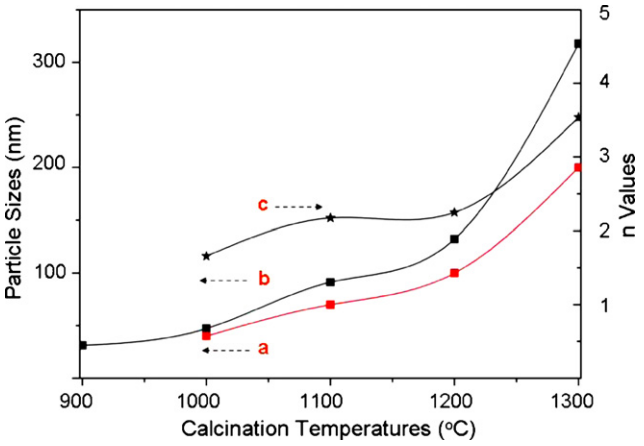

Fig. 4. Variation of D_{sem} (a), D_{bet} (b) and n (c) with calcination temperature.

3.2. Effects of calcination temperature on the characteristics of the powders

As mentioned before, the precursors from the reverse titration co-precipitation process should possess co-precipitation characteristics. Therefore, an investigation of the effect of calcination temperature on the sintering properties of YAG powders was performed on the YAG precursors obtained by the same process as with set 2.

Fig. 2 shows the XRD patterns of the powders calcined at the temperatures in range of 900–1300 °C for 2 h. All the peaks of the product calcined at 900 °C correspond to the characteristic peaks of cubic YAG (JCPDS card No. 72-1315). As is well known, secondary phases, especially hexagonal $YAlO_3$ (h-$YAlO_3$), often appears as

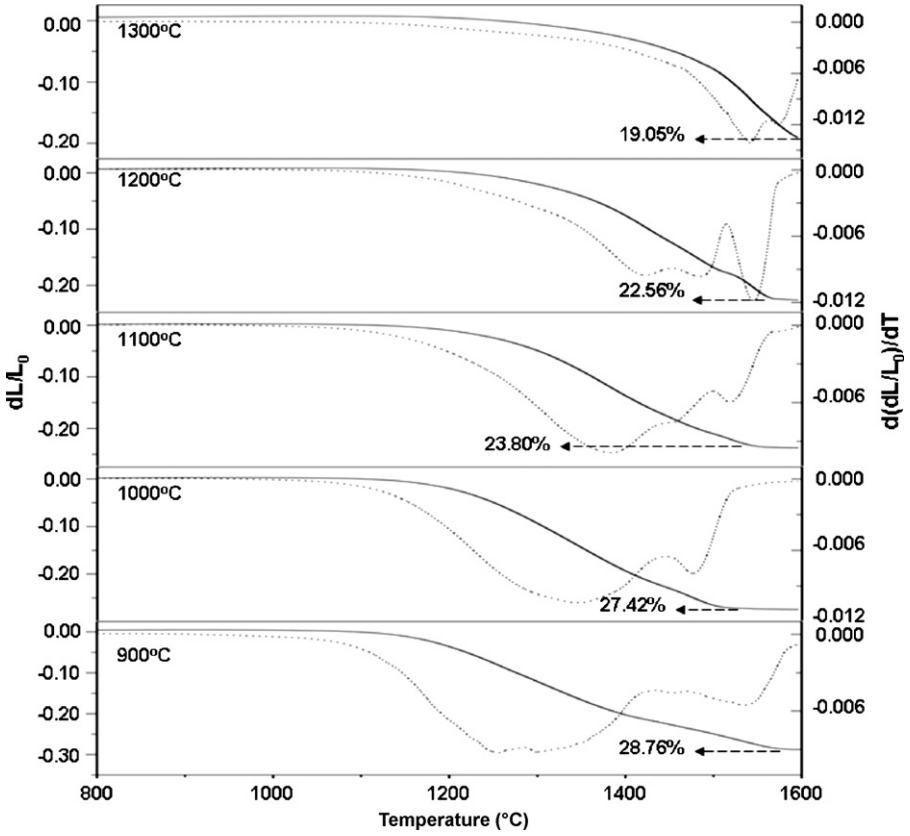

Fig. 5. Linear shrinkage of compacts made from powder calcined at different temperatures.

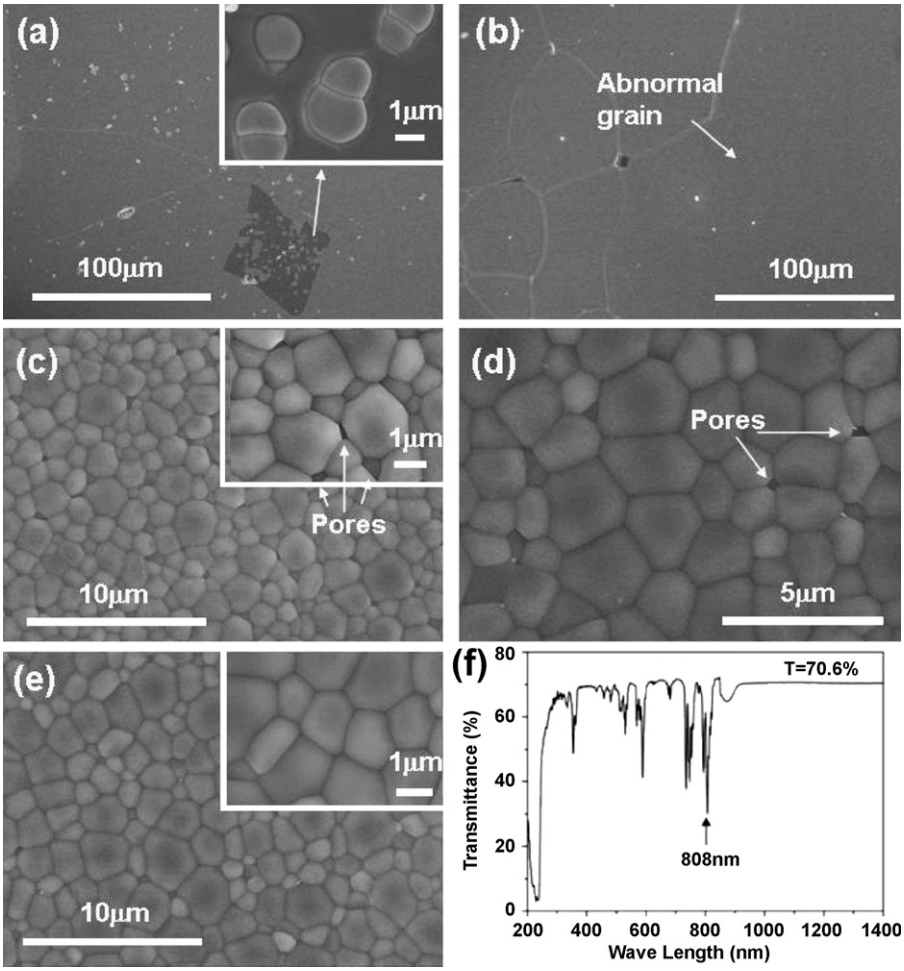

Fig. 6. SEM images of grains in ceramics made from the powder obtained by calcination at different temperatures: (a) 900 °C, (b) 1000 °C, (c) 1100 °C, (d) 1200 °C, (e) 1300 °C; (f) transmittance of sample-e.

intermediate products during YAG synthesis using the wet chemistry method [28,30–32]. However, it was not found in this work. These results show that the distribution of yttrium and aluminum compounds in the YAG precursor synthesized via the reverse titration co-precipitation method is homogeneous. The XRD pattern of the product calcined at temperatures over 900 °C also corresponds to those of the pure YAG phases.

The morphology of the powders calcined for 2 h at different temperatures is exhibited in Fig. 3. The particles appear somewhat merged together. The primary particles grow with an increase in the calcination temperatures. Fig. 3(a) and (b) shows FESEM and TEM images of the samples calcined at 900 °C, respectively. The powder calcined at 900 °C exhibits poor crystallization with irregular morphology and non-uniform particle size. From Fig. 3(c–f), it is seen that the particles of the samples calcined at the higher temperatures of 1000, 1100, 1200, and 1300 °C are well crystallized and merge together forming a dendritic agglomeration. The morphologies of these samples are similar among each other, except that the size of the particles increases with increasing calcination temperature. From the images, the average particle diameters are about 40, 50, 100, and 200 nm, respectively.

The BET surface areas of the powders calcined at temperatures ranging from 900 to 1300 °C are 42.15, 27.91, 14.43, 9.97 to 4.15 m^2/g, respectively. The average particle size D_{bet}, which is calculated from the relationship $D_{bet} = 6/\rho S_{bet}$ (where $\rho = 4.55\ g/cm^3$), exhibits a ten-fold increase from 31.28 nm to 317 nm. Using the average diameters (D_{sem}) obtained from the SEM images, the relationship between D_{bet} and D_{sem} is illustrated in Fig. 4. In order to describe the degree of dendritic agglomeration, a parameter n is introduced, which represents the number of particles that are merged together. Physical meaning of n is that it approximately equal to the slenderness ratio of an agglomeration containing several particles. The n value is calculated using the equation: $n = \frac{R_{bet}^2 - R_{xrd}^2}{R_{xrd}^2 \cos\theta} + 1$, where D_{sem}. $\sin\theta$ is the diameter of the linkage neck of adjacent particles, and $D = 2R$. From statistics on the diameters of the linkage necks of the particles, $\cos\theta$ is chosen to be equal to 0.6. Curves (a) and (b) show the respective variation of D_{sem} and D_{bet}. The values are comparable at 1000, 1100 and 1200 °C, but some deviation occurs at 1000 or at 1300 °C. The deviation indicates a change in the relationship between D_{sem} and D_{bet}, which is illustrated by the variation of n in curve (c). The n values corresponding to samples calcined at 1100 and 1200 °C are similar, while the n values related to the samples calcined at 1000 and 1300 °C are remarkably different.

Fig. 5 shows the shrinkage behavior of the compacts made from the powder calcined at different temperatures. For the sample calcined at 900 °C, apparent densification begins at around 950 °C, and the total linear shrinkage is 28.76%. With an increase in the calcination temperature, the onset of densification postpones, and the total linear shrinkage of the samples decreases. When the calcination temperature approaches 1300 °C, densification begins at a temperature of over 1300 °C, and the total linear shrinkage is 19.05%, with a narrow temperature range for densification. The total linear

shrinkages of the samples calcined at 900 and 1000 °C, as well as those calcined at 1100 and 1200 °C, exhibit comparable values to each other. The linear shrinkage of the powder calcined at 1000 and 1100 °C, as well as those calcined at 1200 and 1300 °C exhibit deviation. This result is in accordance with the variation of *n* analyzed from the SEM and BET measurements. From these results, we infer that the effective interval for calicination is about 200 °C between 900 and 1300 °C.

SEM images of the polished and thermal-etched ceramics prepared from the above powder samples after sintering in vacuum at 1700 °C for 10 h are shown in Fig. 6(a–e). The transmittance of the ceramics made from powders calcined at 1300 °C is shown in Fig. 6(f). Observed grain boundaries are rare in the sample made from the powder calcined at 900 °C in Fig. 6(a). There is a different region with a deep color wrapped inside the grain. In an enlarged image (inset in Fig. 6(a)), many isolated small grains of several microns in size are apparent. The formation of this secondary phase region and the abnormal grain growth is caused by low-crystallinity and the extremely high sintering activity of the nano-powders obtained by calcination at the low temperature of 900 °C only. Fig. 6(b) exhibits a better view of a grain boundary, while the abnormal grain growth in the sample is also apparent. The sample is sintered from the powder obtained by calcination at 1000 °C. Similar to the sample calcined at 900 °C, it has comparable sintering activity (similar BET surface areas), which causes the sintering process to go out of control. However, it has better crystallinity, and the grain boundaries are much cleaner. Fig. 6(c–e) exhibits grains of the ceramics obtained from the powder obtained by calcination at 1100, 1200, and 1300 °C, respectively. They exhibit similar features for the grains and the grain boundaries. The grain size ranges from 0.5 to 3 μm, much smaller than those of the ceramics made via solid-reaction [2,33]. According to Mie theory, when the grain size is equal to the wavelength, the transmittance should be low. However, Yagi et al. report that ceramics with an average grain size of about 1.5 μm are highly transparent, and can realize laser oscillation [34,35]. Fedyk et al. have obtained transparent YAG ceramics with an average grain size about 500 nm using a high-pressure low temperature sintering technique (HPLT) by applying a super-high pressure of 8 GPa at 450 °C [36]. As Ikesus et al. concluded, grain boundaries appear to do little harm to the transmittance [2]. The main scattering factors are secondary phases as well as residual pores. So, although small grains introduce more grain boundaries, the ceramics still has an excellent quality sufficient to realize laser oscillation, as long as it is clean enough. The density of the residual pores in the images decreases from Fig. 6(c) to (e). The grain boundaries are almost clean, and the sintering aid of SiO_2 has not separated out. The transmittance of the ceramic, which was fabricated with the powder calcined at 1300 °C without further polishing is exhibited in Fig. 6(f). The transmittance in the infrared region is over 70%. The characteristic absorption peak at 808 nm of neodymium ions is evident.

The sintering activity of all the prepared powders provides enough energy for the ceramics to achieve full densification. However, when the powder has excessive energy for sintering, the grains grow out of control during the sintering process. This situation leads to abnormal grain growth, and it is easy to form closed pores in the samples, as shown in Fig. 6(a and b). In Fig. 6(c–e), the powder samples calcined at 1100 °C and above exhibit moderate sintering activity. The grains grow steadily and homogeneously with the help of SiO_2 as a sintering aid [37–39]. The effect of the sintering aid is not only to lower the sintering temperature, but also to restrain boundary growth which allows enough passages for the pores to diffuse out of the body. The pores can only diffuse using the grain boundaries as channels. In order to reduce the number of defects, such as bubbles or secondary phases, the grains need to grow slowly, and have sufficient boundaries remaining before the ceramic approaches full-density [34]. So the powder obtained at temperatures lower than 1100 °C is not suitable for the fabrication of transparent ceramics.

4. Conclusions

Different titration co-precipitation methods for the synthesis of YAG precursors with nitrates and ammonium hydrogen carbonate were studied. The results indicate that the Al-precipitate forms first, and the Y-precipitate forms later during the normal titration co-precipitation process. This order results from the pH not reaching the solubility product value of Y^{3+}. The Y/Al ratio in the precipitate changes from a low value to the stoichiometric ratio. However, in the co-precipitation process by reverse titration method, the Y- and Al- precipitates formed simultaneously with a stable Y/Al ratio in the precipitate near the stoichiometric value. Considering the droplet and its neighborhood to be a micro-reactor, the precipitation process at this location should be similar to that of a normal titration process. Thus, precipitate made by the reverse titration method is assumed to consist of core–shell microstructure. The above facts imply that the formation process of precipitate obtained by reverse titration process is assembled with numbers of micro-reaction process, which is like the one obtained by normal titration process.

Precursors made by the reverse titration co-precipitation method can form pure YAG phases by calcination even at the low temperature of 900 °C. Compared with the shrinkage characteristics of the compacts made from the powder obtained by calcination at different temperatures, the densification of the compact made from the powder calcined at 900 °C begins at a temperature of about 300 °C lower than that made from the powder calcined at 1300 °C, and the total shrinkage ratio is also about 30% higher. These results indicate that the powder obtained at the lower temperature has excessively high sintering activity, which leads to an uncontrollable sintering process. The sintering results prove that the samples made from the powder calcined at low temperatures readily exhibit abnormal grain growth and pore envelopment; while those made from the powder calcined at high temperatures produce a uniform grain distribution, fewer residual pores and high transmission, even though the particle size reaches 200 nm with some agglomeration.

Acknowledgements

This work was supported by NSFC (Nos. 50990303, 50925205, 50872070, and 5070231), 973 program (2010CB833103), and the Program of Introducing Talents of Discipline to Universities (111 Program: b06015).

References

[1] T. Sekino, Y. Sogabe, Rev. Laser Eng. 21 (8) (1993) 827–831.
[2] A. Ikesue, T. Kinoshita, K. Kamata, K. Yoshida, J. Am. Ceram. Soc. 78 (1995) 1033–1040.
[3] S.A. Hassanzadeh-Tabrizi, E. Taheri-Nassaj, H. Sarpoolaky, J. Alloys Compd. 456 (2008) 282–285.
[4] Y.P. Fu, S.B. Wen, C.S. Hsu, J. Alloys Compd. 458 (2008) 318–322.
[5] M.L. Saladino, G. Nasillo, D.C. Martino, E. Caponetti, J. Alloys Compd. 491 (2010) 737–741.
[6] D.J. Sordelet, M.L. Akinc, Y. Han, M.H. Han, J. Eur. Ceram. 14 (1994) 123–130.
[7] J.G. Li, X.D. Li, X.D. Sun, T. Ikegami, T. Ishigaki, Chem. Mater. 20 (2008) 2274–2281.
[8] X. Li, H. Liu, J.Y. Wang, F. Han, R.I. Boughton, J. Am. Ceram. Soc. 87 (2004) 2288–2290.
[9] X. Li, H. Liu, J.Y. Wang, H.M. Cui, F. Han, X.D. Zhang, R.I. Boughton, Mater. Lett. 58 (2004) 2377–2380.
[10] Z.G. Wu, X.D. Zhang, W. He, Y.W. Du, N.T. Jia, P.C. Liu, F.Q. Bu, J. Alloys Compd. 472 (2009) 576–580.
[11] N.T. Jia, X.D. Zhang, W. He, W.J. Hu, X.D. Meng, Y. Du, J.C. Jiang, Y.W. Du, J. Alloys Compd. (2010), doi:10.1016/j.jallcom.2010.071.

[12] J.H. In, H.C. Lee, M.J. Yoon, K.K. Lee, J.W. Lee, C.H. Lee, J. Supercrit. Fluids 40 (2007) 389–396.
[13] M. Danchevskaya, Y. Ivakin, S. Torbin, G. Muravieva, J. Supercrit. Fluids 46 (2008) 358–364.
[14] Q.X. Zheng, B. Li, H.D. Zhang, J.J. Zheng, M.H. Jiang, X.T. Tao, J. Supercrit. Fluids 50 (2009) 77–81.
[15] T. Yanagitani, H. Yagi, M. Ichikawa, Japanese patent: 10–101333 (1997).
[16] T. Yanagitani, H. Yagi, Y. Hiro, Japanese patent: 10–101411 (1998).
[17] H. Yagi, T. Yanagitani, K. Takaichi, K.I. Ueda, A.A. Kaminskiim, Opt. Mater. 29 (2007) 258–262.
[18] X. Li, Q. Li, J.Y. Wang, S.L. Yang, H. Liu, Opt. Mater. 29 (2007) 528–531.
[19] H. Gong, D.Y. Tang, H. Huang, J. Ma, J. Am. Ceram. Soc. 92 (2009) 812–817.
[20] Z.H. Chen, Y. Yang, Z.G. Hu, J.T. Li, S.L. He, J. Alloys Compd. 33 (2007) 328–331.
[21] A.K. Pradhan, K. Zhang, G.B. Loutts, Mater. Res. Bull. 39 (2004) 1291–1298.
[22] J.G. Li, T. Ikegami, J.H. Lee, T. Mori, Y. Yajima, J. Eur. Ceram. Soc. 20 (2000) 2395–2405.
[23] Z.H. Wang, L. Gao, J. Inorg. Mater. 16 (4) (2001) 630–634.
[24] W.B. Liu, W.X. Zhang, J. Li, H.M. Kou, Y.Q. Shen, L. Wang, Y. Shi, D. Zhang, Y.B. Pan, J. Alloys Compd. 503 (2010) 525–528.
[25] Y.M. Zhang, H.M. Yu, Ceram. Int. 35 (2009) 2077–2081.
[26] R. Singh, R.K. Khardekar, A. Kumar, D.K. Kohli, Mater. Lett. 61 (2007) 921–924.
[27] J. Li, Y.B. Pan, F. Qiu, Y.S. Wu, W.B. Liu, J.K. Guo, Ceram. Int. 33 (2007) 1047–1052.
[28] N. Matsushita, N. Tsuchiya, K. Nakatsuka, T. Yanagitani, J. Am. Ceram. Soc. 82 (8) (1999) 1977–1984.
[29] J.G. Li, T. Ikegami, J.-H. Lee, Y. Mori, Y. Yajima, J. Mater. Res. 15 (2000) 1864–1867.
[30] P. Palmero, C. Esnouf, L. Montanaro, G. Fantozzi, J. Eur. Ceram. Soc. 25 (2005) 1565–1573.
[31] P. Palmero, L. Montanaro, J. Therm. Anal. Calorim. 88 (1) (2007) 261–267.
[32] N.J. Hess, G.D. Maupin, L.A. Chick, D.S. Sunberg, D.E. Mccreedy, T.R. Armstrong, J. Mater. Sci. 29 (1994) 1873–1878.
[33] L. Esposito, A. Piancastelli, J. Eur. Ceram. Soc. 29 (2009) 317–322.
[34] H. Yagi, K. Takaichi, K. Ueda, Y. Yamasaki, T. Yanagitani, A.A. Kaminskii, Laser Phys. 15 (9) (2005) 1338–1344.
[35] K. Ueda, J.F. Bisson, H. Yagi, K. Takaichi, A. Shirakawa, T. Yanagitani, A.A. Kaminskii, Laser Phys. 15 (7) (2005) 927–938.
[36] R. Fedyk, D. Hreniak, W. Lojkoski, W. Strek, H. Matysiak, E. Grzanka, S. Gierlotka, P. Mazur, Opt. Mater. 29 (2007) 1252–1257.
[37] S. Kochawattana, A. Stevenson, S.H. Lee, M. Ramirez, V. Gopalan, J. Dumm, V.K. Castillo, J. Eur. Ceram. Soc. 28 (2008) 1527–1534.
[38] R. Boulesteix, A. Maitre, J.F. Baumarda, Y. Rabinovitch, C. Salle, S. Weber, M. Kilo, J. Eur. Ceram. Soc. 29 (2009) 2517–2526.
[39] Y.K. Li, S.M. Zhou, H. Lin, X.R. Hou, W.J. Li, H. Teng, T.T. Jia, J. Alloys Compd. 502 (2010) 225–230.